

# XOR-Ising Loops and the Gaussian Free Field

David B. Wilson

Microsoft Research, Redmond, WA 98052, USA

(Dated: February 18, 2011)

We find by simulation that the interfaces in the exclusive-or (XOR) of two independent 2D Ising spin configurations at the critical temperature form an ensemble of loops that have the same distribution as the contour lines of the Gaussian free field, but with the heights of the contours spaced  $\sqrt{2}$  times as far apart as they are for the conformal loop ensemble  $CLE_4$  or the double dimer model on the square lattice. For domains with boundary, various natural boundary conditions for the two Ising models correspond to certain boundary heights for the Gaussian free field.

## XOR-ISING LOOPS AND RELATED MODELS

The double-Ising model consists of two independent Ising spin configurations  $\sigma$  and  $\tau$  on the same graph. The double-Ising model on planar graphs is closely related to a variety of statistical physics models, including the Ashkin-Teller model [1, 2], the 8-vertex model [1, 2], the Gaussian model [3–8], the double-dimer model, and spanning trees [9, 10], some of which we discuss below. The XOR-Ising configuration  $\xi$  (illustrated in Figure 1) is defined by  $\xi_v = \sigma_v \times \tau_v$  for each vertex  $v$  of the graph (if the spin values are  $\pm 1$ ), or equivalently,  $\xi_v = \sigma_v \oplus \tau_v$  (if the spin values are false and true), where  $\oplus$  denotes exclusive-or (XOR). The XOR-Ising spins  $\xi$  also called the polarization of the double-Ising model [3]. The interfaces between  $+1$  spins and  $-1$  spins in an XOR-Ising configuration form loops or paths connecting boundary points. We find empirically that when the two Ising models are at the critical temperature, the XOR-Ising loops are closely related to contour lines of a Gaussian free field, but that, in a sense that we will make more precise, there are fewer XOR-Ising loops than loops in other loop models that are related to the Gaussian free field.

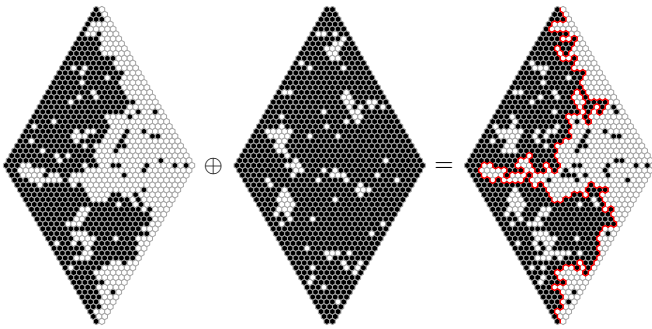


FIG. 1. (Color online) On the left is the critical Ising model on a lozenge-shaped domain of order  $L = 32$  with black-white boundary conditions. The interface from bottom to top is in the scaling limit  $SLE_3$  [11, 12]. In the middle is the critical Ising model with black boundary conditions. The ensemble of loops is in the limit  $CLE_3$  [11, 12]. On the right is the XOR of the left and middle spin configurations. The interface from bottom to top appears to be  $SLE_{4, \sqrt{2}-1, \sqrt{2}-1}$  in the scaling limit.

XOR-Ising interfaces are (essentially) the same as the double-dimer model on the Fisher lattice, as we now explain. A dimer configuration on a graph is a pairing of the vertices such that every vertex is paired with exactly one of its neighbors. Fisher showed that the Ising model on any graph has the same partition function as dimer configurations on a related graph [13]. This relation is not combinatorial, but for *planar* graphs there is a combinatorial correspondence between dimers and Ising spins, based on the Ising model's low temperature expansion [1]. When the Ising spins are on the triangular lattice, the dimer configurations are on a graph consisting of dodecagons and triangles, called the Fisher lattice.

The double-dimer model is formed by superimposing two independent random dimer configurations; the result is a collection of loops and doubled edges. If one of the dimer configurations has two defects (monomers) on the boundary, then the double-dimer configuration also has a path connecting the defects. If we ignore the route that a double-dimer loop (on the Fisher lattice) takes within the triangles, the double-dimer loop traces out a path where one Ising configuration has aligned spins while the other one does not. Then double-dimer loops on the Fisher lattice (ignoring doubled edges and the intratriangle portions of loops) are just the XOR-Ising interfaces.

It is instructive to compare XOR-Ising loops with the double-dimer model on other lattices. On the square lattice or hexagonal lattice with suitable boundary conditions, the scaling limit of a double-dimer path connecting two boundary points is conformally invariant [14] and is thought to be described by Schramm-Loewner evolution with parameter 4 ( $SLE_4$ ) (see e.g., [15–17]). The scaling limit of the whole ensemble of loops is conjectured to be the conformal loop ensemble with parameter 4 ( $CLE_4$ ) [18]. (The conformal loop ensemble  $CLE_\kappa$  is thought to be the scaling limit of the  $O(n)$  model when  $n = -2 \cos(4\pi/\kappa)$  [18].) Dimer configurations on the square and hexagonal lattices have height functions that are known to behave like the Gaussian free field in the scaling limit [19, 20], and  $CLE_4$  is known to be the scaling limit of contour lines of the Gaussian free field where the heights of the contours are separated by a certain spacing [21]. But the techniques for analyzing the double-dimer model [14] depend in an essential way upon the lattice

quantity	XOR-Ising loops	nearly exact value	CLE <sub>4</sub> loops (exact value)
loop dimension	$1.5000 \pm 0.0003$	$1.5000 \dots = 3/2$	$1.5000 \dots = 3/2$
winding angle variance / $\log L$	$1.0000 \pm 0.0003$	$1.0000 \dots = 1$	$1.0000 \dots = 1$
$E[\# \text{ loops around point}] / \log L$	$0.07168 \pm 0.00005$	$0.07164 \dots = 1/(\sqrt{2}\pi^2)$	$0.10132 \dots = 1/\pi^2$
$\text{Var}[\# \text{ loops around point}] / \log L$	$0.05057 \pm 0.00003$	$0.05066 \dots = 1/(2\pi^2)$	$0.06755 \dots = 2/(3\pi^2)$
gasket dimension	$1.91400 \pm 0.00006$	$1.91421 \dots = 1/2 + \sqrt{2}$	$1.87500 \dots = 15/8$
electrical thickness	shown in Fig. 2	excursion time of BM from $[-\pi, \pi]$	excursion time of BM from $[-\pi, \pi]$
difference in log conformal radii	shown in Fig. 3	exit time of BM from $[-\pi, \sqrt{2}\pi]$	exit time of BM from $[-\pi, \pi]$

TABLE I. Comparison of XOR-Ising loops with the conformal loop ensemble CLE<sub>4</sub>. The (first five) measured values are from configurations on  $L \times L$  tori for  $L = 2^{10}, 2^{11}, 2^{12}$ . The properties of individual XOR-Ising loops appear to be the same as for CLE<sub>4</sub> loops, but the two loop ensembles are different. The measured values of the XOR-Ising loops are consistent with contour lines of the Gaussian free field, but with height differences between contours being  $\sqrt{2}$  times as large as for CLE<sub>4</sub>.

being bipartite, which the Fisher lattice is not. Dimers on the Fisher lattice have no height function, and the monomer correlations for the Fisher lattice [22, 23] behave quite differently from monomer correlations on the square and hexagonal lattices [24]. Nonetheless, as we shall see, individual double-dimer loops on the critical Fisher lattice appear to have the same limiting behavior as loops of the square- or hexagonal-lattice double-dimer models, but there are  $\sqrt{2}$  times fewer loops in the Fisher-lattice double-dimer model.

The polarization of the double-Ising model (the XOR-Ising configuration) at the critical temperature has been identified with a “spin wave operator” of the Gaussian free field [3] (see also [4–8]), and this identification has been used to compute Ising spin correlations [22, 23]. However, the focus was on correlation functions, and it is unclear how to use these works to extract information about the geometric properties of XOR-Ising interfaces.

Boutillier and de Tilière [9, 10] studied the partition function of the double-Ising model on “isoradial” graphs, which include the hexagonal and square lattices. They showed that when the Ising models are critical, the partition function is identical to the partition function for cycle-rooted spanning forests on the same graph. Spanning trees can be transformed into dimers on a related bipartite graph [25, 26], which have a height function whose scaling limit is the Gaussian free field. However, there is no known algorithm for transforming cycle-rooted spanning forests to pairs of Ising spin configurations, so it is not clear how to use their results to relate the Gaussian free field to XOR-Ising interfaces.

Sheffield and Werner gave a characterization of the conformal loop ensemble CLE <sub>$\kappa$</sub>  for  $8/3 < \kappa \leq 4$ . The gasket is the set of points not surrounded by any loop of CLE <sub>$\kappa$</sub> . Sheffield and Werner showed that the CLE <sub>$\kappa$</sub>  gasket is the same as the set of points not surrounded by any loop of the Brownian loop soup with intensity  $c = (3\kappa - 8)(6 - \kappa)/(2\kappa)$  (the central charge) [27]. Since  $c(\kappa = 3) = \frac{1}{2}$  and  $c(\kappa = 4) = 1$ , the intersection of two independent CLE<sub>3</sub> gaskets is a CLE<sub>4</sub> gasket. It follows im-

mediately that the gasket for the OR (rather than XOR) of two independent critical Ising models is the same as the CLE<sub>4</sub> gasket [28], which is the scaling limit of contour lines of the Gaussian free field. It is not clear, however, how to relate the OR-Ising loops to the XOR-Ising loops.

## XOR-ISING LOOPS IN THE BULK

We generated many XOR-Ising configurations on large  $L \times L$  tori and measured various properties of the XOR-Ising loop ensemble (see Table I) whose values are known for CLE <sub>$\kappa$</sub> . These include the length of the longest loop (to measure the loop dimension [29]), the winding angle variance of the longest loop [30, 31], the average number of loops surrounding a point [32, 33], the variance in the number of loops surrounding a point [33, 34], and the number of points surrounded by no loops (to measure the gasket dimension [33, 35]). The first two quantities are properties of individual loops, and match the values for CLE<sub>4</sub> loops. The latter three quantities are properties of the ensemble rather than individual loops, and these do *not* match the values for the CLE<sub>4</sub> ensemble. For example, the number of XOR-Ising loops surrounding a point is smaller by a factor of  $\sqrt{2}$  than the number of CLE<sub>4</sub> loops surrounding a disk of radius  $1/L$ .

In view of the various connections between the double-Ising model and the Gaussian free field, and the close match between the measured properties of individual XOR-Ising loops and CLE<sub>4</sub> loops, a natural hypothesis is that the XOR-Ising loops are distributed according to contour lines of the Gaussian free field, but with the height spacing between contours larger than what it would be for CLE<sub>4</sub> loops. To test this, we measured the electrical properties of the XOR-Ising loops.

Consider the surface of a cylinder of length  $\ell \gg 1$ , radius 1, and girth  $2\pi$  made of a resistive medium with resistance  $2\pi$ . Suppose there is a sequence of noncontractible loops  $\mathcal{L}_1, \dots, \mathcal{L}_k$  that wind around the short direction of the cylinder. Let  $R_-(\mathcal{L}_i)$  and  $R_+(\mathcal{L}_i)$  denote

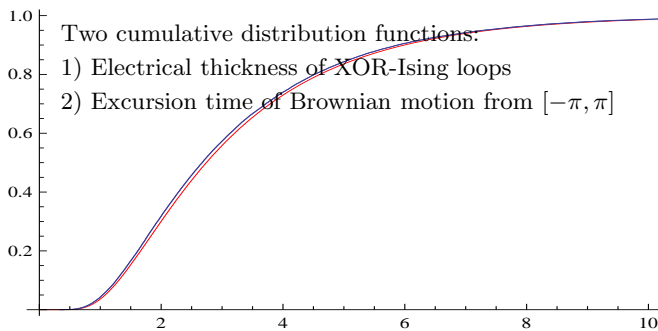


FIG. 2. The electrical thickness of XOR-Ising loops closely matches the Brownian excursion time from  $[-\pi, \pi]$ .

the electrical resistances between loop  $\mathcal{L}_i$  and the left and right ends of the cylinder respectively. If the loops  $\mathcal{L}_1, \dots, \mathcal{L}_k$  are  $\text{CLE}_4$  loops, then  $R_-(\mathcal{L}_{i+1}) - R_-(\mathcal{L}_i)$  is distributed according to the exit time of a standard Brownian motion from the interval  $[-\pi, \pi]$  [33, 34], and in [34] it was predicted that the electrical thickness  $\ell - (R_-(\mathcal{L}_i) + R_+(\mathcal{L}_i))$  of loops  $\mathcal{L}_i$  far from either end of cylinder is distributed according to the *excursion* time of a standard Brownian motion from the interval  $[-\pi, \pi]$ . Schramm and Sheffield proved that  $\text{CLE}_4$  is the scaling limit of the contour lines of the Gaussian free field with a certain spacing  $\lambda$  between the contour heights [21]. It also follows from their work that when the height spacing of the contours is  $x\lambda$ , then  $R_-(\mathcal{L}_{i+1}) - R_-(\mathcal{L}_i)$  is distributed according to the exit time of standard Brownian motion from the asymmetric interval  $[-\pi, x\pi]$  [21, 28]. For the measured XOR-Ising loop density in Table I, the appropriate value of  $x$  is  $\sqrt{2}$ ; this value is also consistent with the variance and gasket dimension measurements.

We generated many XOR-Ising loop configurations on  $2^7 \times 2^{15}$  cylinders, and using Marshall's Zipper program [36] computed the electrical resistances involving the non-contractible loops. As shown in Figures 2 and 3, there is excellent agreement between the measured distributions and the distributions for contour lines of the GFF with height spacing  $\sqrt{2}$  times as large as for  $\text{CLE}_4$ .

### XOR-ISING INTERFACES IN DOMAINS WITH BOUNDARY

To further test the connection between XOR-Ising interfaces and the Gaussian free field, we measured left-crossing probabilities of the XOR-Ising paths connecting two boundary points of a domain with boundary. Figure 4 illustrates the coordinate  $\theta$  against which we plotted left-crossing probabilities in Figure 5. There are a variety of boundary conditions for the two Ising models that force an interface in the XOR-Ising configuration. For the solid boundary conditions in Figure 1, the left-crossing probabilities of the interface are consistent

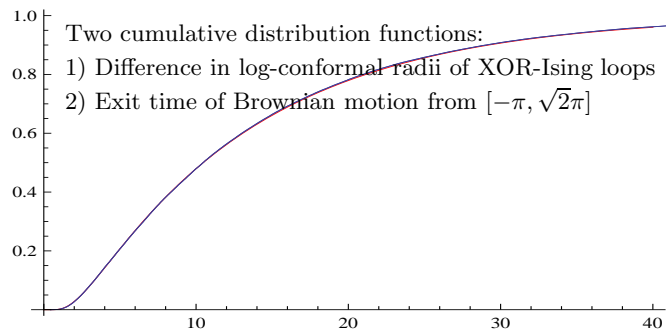


FIG. 3. The difference in log-conformal radii of XOR-Ising loops closely matches the Brownian exit time from  $[-\pi, \sqrt{2}\pi]$ .

with  $\text{SLE}_{4, \sqrt{2}-1, \sqrt{2}-1}$  (see Figure 5), which corresponds to boundary heights of  $\pm\sqrt{2}\lambda$  for the Gaussian free field [21]. If instead the boundary spins alternate between black and white (effectively free boundary conditions), with an interface forced by two phase shifts (see Figure 5), then the left-crossing probabilities are consistent with  $\text{SLE}_{4, -1, -1}$ , which corresponds to boundary heights of  $\pm\varepsilon$  (in the limit  $\varepsilon \downarrow 0$ ) for the Gaussian free field.

We also tried a third set of boundary conditions, which specifies the boundary spin values of neither Ising model, but instead conditions on their forming an interface. We did this by generating Ising spin configurations on a long cylinder with antiperiodic boundary conditions, and taking the two Ising spin configurations from the upper half and lower half of the cylinder. For XOR-Ising interfaces obtained in this way, the left-crossing probabilities are consistent with  $\text{SLE}_{4, 1/\sqrt{2}-1, 1/\sqrt{2}-1}$ . This is somewhat surprising, since these boundary conditions satisfy the domain Markov property at the discrete level, so

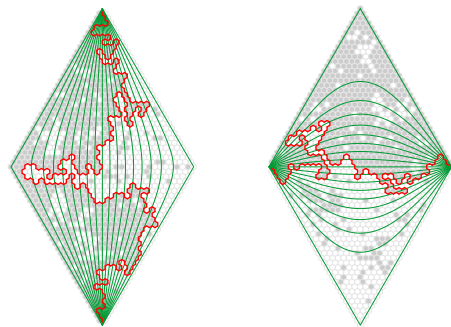


FIG. 4. (Color online) On the left is the XOR-Ising interface from bottom to top from Figure 1; on the right is the corresponding XOR-Ising interface from left to right. When the domain is conformally mapped to the upper half plane with start- and end-points of the interface mapped to 0 and  $\infty$ , the green curves get mapped to rays  $re^{i\theta}$  for constant  $\theta$ . When plotting left-crossing probabilities in Figure 5, for the region on the left we took sites on the short diagonal and compared the site's  $\theta$  with the site's left-crossing probability; for the region on the right we did this for sites on the long diagonal.

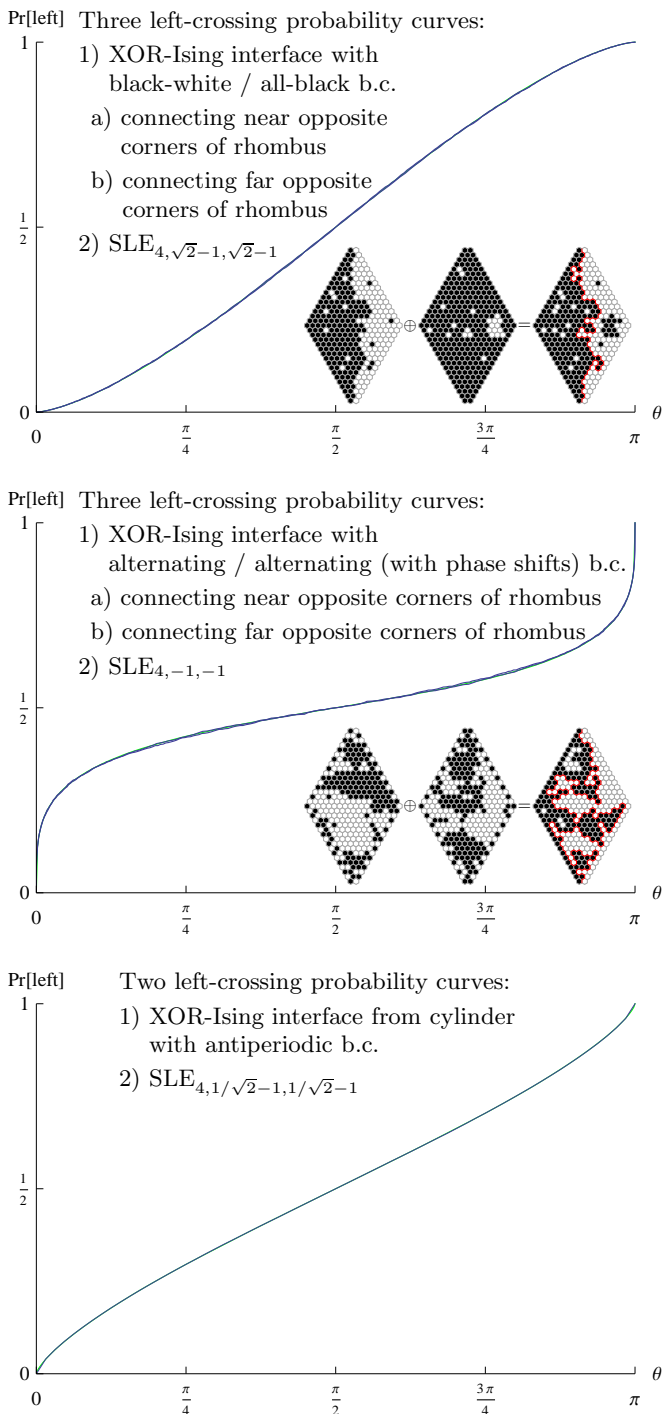


FIG. 5. (Color online) Left-crossing probabilities for XOR-Ising interfaces with different boundary conditions and different geometries, compared with the left-crossing probabilities for  $SLE_{4,\rho,\rho}$  for different  $\rho$ 's. (The top, middle, and bottom plots show 3 curves, 3 curves, and 2 curves, respectively; in each plot the curves are essentially indistinguishable.) The geometry of the domain appears not to matter, consistent with conformal invariance of the XOR-Ising interfaces. Different boundary conditions correspond to different  $\rho$ 's. The left-crossing probabilities for  $SLE_{4,\rho,\rho}$  were measured by sampling the left-crossing probabilities of a contour line in a Gaussian free field with  $\pm(1+\rho)\lambda$  boundary conditions [21].

one might expect the interface to be simply  $SLE_4$ . But evidently these boundary conditions act differently on smooth boundaries than they do on rough boundaries.

We thank Scott Sheffield, Gady Kozma, and Bernard Nienhuis for useful discussions.

- 
- [1] R. J. Baxter, *Exactly solved models in statistical mechanics* (Academic Press, London, 1982) pp. xii+486.
- [2] B. Nienhuis, in *Phase transitions and critical phenomena, Vol. 11* (Academic Press, London, 1987) pp. 1–53.
- [3] L. P. Kadanoff and A. C. Brown, *Ann. Physics* **121**, 318 (1979).
- [4] H. J. F. Knops, *Ann. Physics* **128**, 448 (1980).
- [5] H. J. Hilhorst and J. M. J. van Leeuwen, *Phys. A* **106**, 301 (1981).
- [6] P. Di Francesco, H. Saleur, and J.-B. Zuber, *Nuclear Phys. B* **290**, 527 (1987).
- [7] D. Boyanovsky, *Nuclear Phys. B* **5**, 20 (1988).
- [8] D. Boyanovsky, *Phys. Rev. B* (3) **39**, 6744 (1989).
- [9] C. Boutillier and B. de Tilière, *Probab. Theory Related Fields* **147**, 379 (2010), arXiv:0812.3848.
- [10] B. de Tilière, (2010), arXiv:1012.4836.
- [11] S. Smirnov, *Ann. of Math. (2)* **172**, 1435 (2010).
- [12] D. Chelkak and S. Smirnov, (2009), arXiv:0910.2045.
- [13] M. E. Fisher, *J. Math. Phys.* **7**, 1776 (1966).
- [14] R. Kenyon, (2011), manuscript.
- [15] S. Rohde and O. Schramm, *Ann. of Math. (2)* **161**, 883 (2005), math/0106036.
- [16] O. Schramm, in *International Congress of Mathematicians. Vol. I* (2007) pp. 513–543, math/0602151.
- [17] J. Cardy, *Ann. Physics* **318**, 81 (2005).
- [18] S. Sheffield, *Duke Math. J.* **147**, 79 (2009), math/0609167.
- [19] R. Kenyon, *Ann. Probab.* **29**, 1128 (2001).
- [20] R. Kenyon, *Comm. Math. Phys.* **281**, 675 (2008).
- [21] O. Schramm and S. Sheffield, *Acta Math.* **202**, 21 (2009).
- [22] A. Luther and I. Peschel, *Phys. Rev. B* **12**, 3908 (1975).
- [23] J. L. Richardson and M. Bander, *Phys. Rev. B* **17**, 1464 (1978).
- [24] M. Ciucu, *Mem. Amer. Math. Soc.* **178**, x+144 (2005).
- [25] H. N. V. Temperley, in *Combinatorics: Proc. British Combinatorial Conference 1973* (1974) pp. 202–204.
- [26] R. W. Kenyon, J. G. Propp, and D. B. Wilson, *Electron. J. Combin.* **7**, article #25 (2000), math/9903025.
- [27] S. Sheffield and W. Werner, (2010), arXiv:1006.2373.
- [28] S. Sheffield, Personal communication.
- [29] V. Beffara, *Ann. Probab.* **36**, 1421 (2008).
- [30] B. Wieland and D. B. Wilson, *Phys. Rev. E* **68**, 056101 (2003), arXiv:1002.3220.
- [31] B. Duplantier, in *Les Houches, Session LXXXIII, 2005, Mathematical Statistical Physics* (Elsevier, 2006) pp. 101–217, math-ph/0608053.
- [32] J. Cardy and R. M. Ziff, *J. Statist. Phys.* **110**, 1 (2003).
- [33] O. Schramm, S. Sheffield, and D. B. Wilson, *Comm. Math. Phys.* **288**, 43 (2009), math.PR/0611687.
- [34] R. W. Kenyon and D. B. Wilson, (2004), manuscript.
- [35] B. Duplantier, *Phys. Rev. Lett.* **64**, 493 (1990).
- [36] D. E. Marshall and S. Rohde, *SIAM J. Numer. Anal.* **45**, 2577 (2007), zipper program at <http://www.math.washington.edu/~marshall/zipper.html>.